Q. J. R. Meteorol. Soc. (2004), **130**, pp. 2087–2103 doi: 10.1256/qj.03.161

Flux–gradient relationship, self-correlation and intermittency in the stable boundary layer

By CHERYL L. KLIPP and LARRY MAHRT*
Oregon State University, Corvallis, USA

(Received 21 August 2003; revised 3 March 2004)

SUMMARY

The correlation between dimensionless shear ϕ_m and dimensionless height z/L, where L is the Obukhov length, for stable conditions is strongly influenced by self-correlation for the present datasets. This effect is quite large for stronger stability but still significant for near-neutral conditions. A conditional analysis of nocturnal stable boundary-layer data, where 'non-turbulent' parts of the record are removed, reduces the impact of non-stationarity and therefore reduces the scatter. The conditional analysis also reduces the relative importance of self-correlation. Difficulties with estimating self-correlation are also discussed.

KEYWORDS: CASES99 Monin–Obukhov similarity Nocturnal boundary layer z-less similarity

1. INTRODUCTION

Nocturnal surface cooling induces stratification and partial suppression of turbulence. Values of boundary-layer depth range from a few hundred metres thick with strong winds (large shear generation) and cloudy skies, to only a few metres thick with weak winds and clear skies. During stable conditions, intermittent turbulence often develops, where the strength of the turbulence varies between moderate and very weak, typically on time-scales of a few minutes to a few tens of minutes. Some attribute the intermittency to external forcings such as gravity waves (Finnigan and Einaudi 1981), density currents (Soler *et al.* 2002), low-level jets (Banta *et al.* 2002), or other mesoscale phenomena (Sun *et al.* 2002), others to interactions between the turbulence and local mean gradients (Derbyshire 1999). Intermittency is seldom clearly defined and therefore is sensitive to detection criteria.

For strongly stable conditions, where intermittency is common, the flux–gradient relationship shows considerable scatter compared to more weakly stable conditions. Published formulae for the flux–gradient relationship are generally not intended for strongly stable cases, but are none the less used by numerical models for all stabilities.

In addition, the occurrence of the surface friction velocity in both the Obukhov length and the non-dimensional shear may lead to considerable self-correlation. Such self-correlation produces correlation of the same sign as the physically expected correlation for stable conditions and can therefore lead to false confidence in Monin–Obukhov similarity theory. Self-correlation due to a common divisor has been recognized by the statistics community since Karl Pearson first promoted linear correlation as a scientific tool in the late nineteenth century (Aldrich 1995). It has been noted as a problem in the atmospheric boundary-layer community since at least the late 1970s (Hicks 1978a,b) and subsequently pursued by Hicks (1981), Andreas (2002), Mahrt *et al.* (2003) and others. Self-correlation is usually referred to as spurious correlation in the statistics literature. This study uses multiple datasets to examine the role of self-correlation and reconsiders the method for such evaluation.

* Corresponding author: College of Oceanic and Atmospheric Sciences, Oregon State University, Corvallis, OR 97331, USA. e-mail: mahrt@coas.oregonstate.edu

2. Monin–Obukhov similarity theory

The flux–gradient relationship in the surface layer is usually posed in terms of Monin–Obukhov similarity theory . This similarity theory can be derived from the Buckingham Pi groups (Stull 1988; Barenblatt 1996) obtained using $\partial\overline{U}/\partial z$, u_*, $(\overline{w'\theta'})_0$, $g/\overline{\theta}$, and z as the fundamental variables. Here the wind vector is (u, v, w), $\overline{U}$ is the mean wind, z is the instrument elevation, primes indicate deviations from the mean, $u_* = \{(\overline{u'w'})_0^2 + (\overline{v'w'})_0^2\}^{1/4}$ is the friction velocity, $(\overline{w'\theta'})_0$ is the surface heat flux, g is the acceleration due to gravity, and $\overline{\theta}$ is the mean potential temperature. The results are a dimensionless height z/L, where the Obukhov length L is

$$L = -\frac{\overline{\theta}}{\kappa g}\frac{u_*^3}{(\overline{w'\theta'})_0}, \tag{1}$$

and a dimensionless shear

$$\phi_m = \frac{\kappa z}{u_*}\left(\frac{\partial\overline{U}}{\partial z}\right), \tag{2}$$

where κ is the von Karman constant.

One test of Monin–Obukhov similarity theory compliance is whether or not the scaled variables are universal functions and have no additional dependencies on other variables, such as those surveyed by Mahrt *et al.* (2003). Previous observations indicate the non-dimensional shear for stable conditions to be approximately $\phi_m = 1 + \beta(z/L)$ for $z/L > 0$. Published values for β usually fall in the range of 2.5–5.0 and are usually restricted to z/L values less than 2 (e.g. Högström 1988; Sorbjan 1989; Högström 1996; Howell and Sun 1999; Vickers and Mahrt 1999). Holtslag and De Bruin (1988) and Beljaars and Holtslag (1991) propose a nonlinear model for large values of z/L. The relationship between ϕ_m and z/L shows considerable scatter, especially for large positive values of z/L.

The Monin–Obukhov relationship (Eqs. (1) and (2)) becomes local scaling if the heat flux and stress at level z are significantly different from the surface values (Nieuwstadt 1984). When the instrument at level z is in the surface layer, Monin–Obukhov surface-layer scaling and local scaling are approximately the same. If z is above the surface layer, then the fluxes are significantly smaller than surface fluxes and Monin–Obukhov similarity does not apply. Much of the data in this study fall into this category, in which case, Monin–Obukhov similarity theory does not apply and the relationships default to local similarity theory.

3. Data

We analyse data from the main 60 m tower in CASES99 (Poulos *et al.* 2002; Sun *et al.* 2002) in October of 1999 for the nocturnal period 2000–0500 CST (UTC−6 h) and exclude hours when the mean wind is through the tower (205°–335°). The 20 Hz data from sonic anemometers, deployed at 10, 20, 30, 40, 50 and 55 m, are used for this analysis. Additional sonic anemometers at 1.5 and 5.0 m were deployed on a small tower placed 10 m away. Each sonic anemometer recorded three-dimensional winds and sonic virtual temperature. The sonic anemometer at 1.5 m was moved to 0.5 m on 19 October. Propeller anemometers recorded 1 Hz wind data at 15, 25, 35, and 45 m. Conditions range from near-neutral with relatively strong turbulence to very stable with weak turbulence and/or intermittent turbulence.

(*a*) *Flux calculations*

In calculating turbulent fluxes, we must choose an appropriate time-scale over which to compute the means and resulting deviations from the means. If too short a time-scale is chosen, the flux will be underestimated; if too long, the flux will be contaminated by mesoscale fluctuations and therefore large random flux errors. The ideal averaging window for flux calculation depends on the stability and height above ground (Vickers and Mahrt 2003).

Multi-resolution analysis of the CASES99 nocturnal data indicates that 100 s is an acceptable averaging window except for weakly stable conditions (small z/L) where longer windows might be more suitable. The ϕ_m and z/L values for these small z/L data points change by less than 5% when using 100 s windows instead of longer windows (5 min or more) owing to some cancellation of errors associated with underestimation of both $\overline{w'\theta'}$ and u_*. The net error is generally less than the estimated random flux error. For simplicity, a short 100 s window is used throughout this paper to calculate the fluctuations because they provide optimal flux calculations for the more stable conditions (large z/L), the focus of this paper, while having small effect on the weakly stable data. Fluxes are then averaged over one hour to reduce random flux errors.

(*b*) *Gradients*

Estimated vertical gradients of mean wind and temperature profiles are sensitive to the calculation method, especially near the surface. We compare the performance of several methods and find a local fitting technique preferable to more traditional methods of gradient estimation. The mean wind is expected to follow a log-linear profile only in the surface layer. The surface layer, normally considered to be about the lowest 10% of the boundary layer, may be only a few metres deep, or less, for many of the CASES99 profiles (Mahrt and Vickers 2003). A log-linear fit over the entire tower height is inappropriate and does not provide accurate gradient estimates when the surface layer is significantly shallower than the tower height. A log-linear fit over the entire tower height is only slightly improved by removing the surface constraint $\overline{U} = 0$ at $z = z_0 = 3$ cm (Fig. 1(a)). This value for the roughness length was calculated using only data from near-neutral conditions.

A local log-linear fit better approximates the observed profiles (Fig. 1(b)) even though such a function is not theoretically motivated above the surface layer. With the local-fit method, the lowest profile fit uses the mean wind data from levels 1.5 (0.5), 5 and 10 m as well as the surface constraint $\overline{U}(z_0) = 0$. The gradient is evaluated only for the middle levels, 1.5 (0.5) and 5 m. Next, the profile fit is applied to the mean winds from levels 1.5 (0.5), 5, 10, and 20 m and the gradient evaluated for levels 5 and 10 m. The process is sequentially repeated, stepping up the tower one instrument level at a time. A separate fit is made with data from the four propeller anemometers at 15, 25, 35, and 45 m. For this profile fit, the gradient is evaluated for 20, 30 and 40 m.

Gradients calculated as finite difference and also as log-finite difference were found to produce values comparable to the local log-linear fits at instrument levels of 10 m and higher, but not at the lower levels. For these lower levels, the relationship between ϕ_m and z/L using local-fit gradients yields $\phi_m(z/L = 0) = 1.0$. For the same relationship using finite-difference gradients, ϕ_m values can be significantly larger or smaller than 1.0 depending on the instrument level. Log-finite differencing yields values of ϕ_m closer to 1.0 at $z/L = 0$, but still show a bias larger or smaller than 1.0 depending on the height of the lower instrument levels. For this paper, all mean shears and temperature gradients are evaluated with the local log-linear fit method.

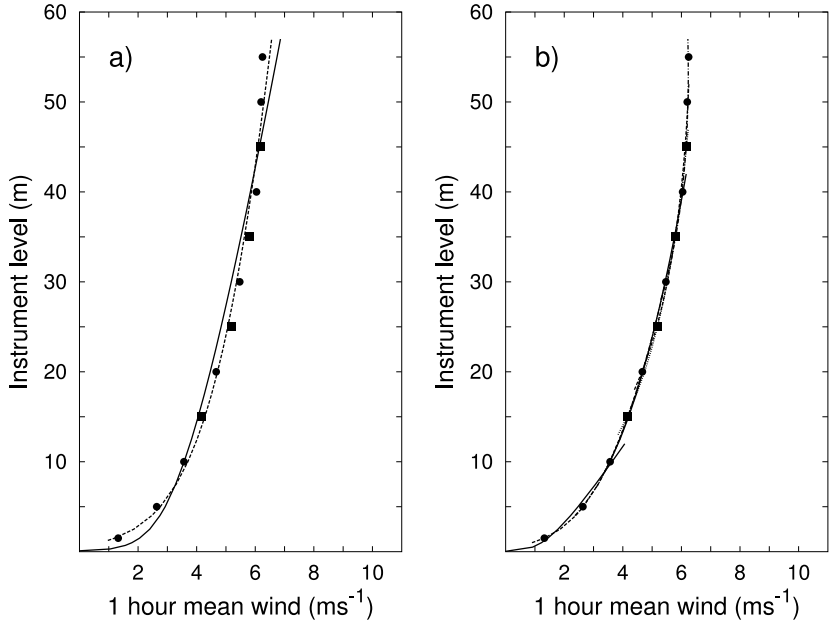

Figure 1. Vertical mean wind profile for 2200–2300 CST (UTC−6 h) 17 October 1999. Circles are sonic anemometer data and squares are propeller data. (a) Traditional log-linear fit, with (—) and without (- -) surface constraint. (b) Local fits to the same data.

TABLE 1. THE LINEAR-CORRELATION COEFFICIENT R BETWEEN ϕ_m AND z/L (SEE TEXT)

Level:	0.5 m	1.5 m	5 m	10 m	20 m	30 m	40 m	50 m
All ϕ_m, $z/L > 0$	0.58	0.90	0.52	0.69	0.79	0.64	0.70	0.35
No weak turbulence	0.75	0.73	0.83	0.85	0.71	0.95	0.92	0.89

4. INFLUENCE OF ELIMINATING VERY WEAK TURBULENCE

Much of the scatter inherent in nocturnal data can be eliminated by omitting hours with weak turbulence and near-zero fluxes or local gradients (Table 1). Although gradients calculated from curves fitted to the wind data are potentially much more accurate than gradients calculated as differences, values of $\partial\overline{U}/\partial z < 0.001\ \mathrm{s}^{-1}$ are indistinguishable from zero. Small flux values are usually characterized by large relative random flux errors (RFE), and may be dominated by mesoscale trend within the averaging window. Using thresholds of standard deviation $\sigma_w = 0.05\ \mathrm{m\ s}^{-1}$, $-\overline{w'\theta'} = 0.001\ \mathrm{m\ K\ s}^{-1}$, and $\partial\overline{U}/\partial z = 0.001\ \mathrm{s}^{-1}$ eliminates all data points with a relative RFE greater than 40% and most data points with relative RFE > 15%. The RFE is calculated as the standard deviation of the thirty-six 100 s fluxes used to calculate the one-hour flux, divided by the square root of 35, that is $\mathrm{RFE} = \sigma_{\mathrm{flux}}/\sqrt{N-1}$, where N is the number of data points. The relative RFE is the RFE divided by the magnitude of the mean flux for that hour.

Application of these thresholds increases the linear-correlation coefficient R between ϕ_m and z/L. However, the linear-correlation coefficient is only a rough relative measure of the scatter in this case since the number of points used to calculate R differs between the set with all of the data and the set with no weak turbulence data. For the 1.5 and 20 m data, the outliers in the full dataset lie far from the main data cluster and

therefore strongly influence the slope of the best-fit line and increase R with respect to the less-scattered no-weak-turbulence data.

Selection of the threshold values for elimination of hours with very weak turbulence is somewhat arbitrary. Setting the limit higher only slightly decreases scatter, but eliminates a large number of data points. Setting the limit lower increases scatter. Since hours with weak turbulence yield highly scattered data, often with large random flux errors for individual records, the following analyses will only use data which satisfy the above thresholds. Additional remaining scatter in extremely stable data may be due to factors not considered here, such as systematic errors in the turbulent fluxes due to flux loss from path length averaging.

5. Sensitivity of linear-correlation coefficient to self-correlation

Both ϕ_m and z/L contain u_* (Eqs. (1) and (2)), causing spurious self-correlation between ϕ_m and z/L. Normally a very small value for the linear-correlation coefficient is considered to indicate no relationship between the variables being compared. When these variables share a common divisor, however, even random data can produce significant non-zero correlation (Kim 1999; Andreas 2002). This 'random' correlation coefficient is a better reference point of no physical relation than $R = 0$.

The degree of self-correlation for data with a common divisor is related to the range and distribution of the values of the fundamental variables. The range and distribution are characterized by the coefficient of variation $V_X = \sigma_X/\overline{X}$ (Kim 1999). Larger coefficients of variation for the common divisor with respect to the coefficients of variation for the other variables lead to larger self-correlation. In this application, σ_X and $\overline{X}$ are the statistics for the whole range of data points collected and should not be confused with the standard deviations used to calculate the uncertainty of individual measurements.

Owing to the dependence of the magnitude of self-correlation on the distribution of the data, it is important that synthesized random data have the same statistical distribution in order to make good comparisons with the actual data. By using randomized actual data to evaluate self-correlation, rather than data synthesized by a random number generator, the range and distribution of the original data are closely reproduced in the random datasets (Kim 1999; Hicks 1978b, 1981).

(*a*) *Random sampling with replacement*

To test the possibility of significant self-correlation, we construct random datasets by using the original observations as a pool of values to draw from at random. For a given z, the fundamental variables that compose ϕ_m and z/L are $\overline{w'\theta'}$, u_* and $\partial\overline{U}/\partial z$. To construct the first random data point for level z, a heat-flux value is chosen at random from the heat-flux data for that level, then a u_* value is chosen at random from the u_* data, and a shear value is chosen at random from the shear data. The process is repeated until the random dataset has as many points as the original data (Fig. 2). Using the random data, new values for ϕ_m and z/L are computed and the linear-correlation coefficient between them is computed (Mahrt *et al.* 2003). This process is repeated 1000 times, that is, 1000 different random sets of data are constructed and 1000 correlation coefficients are calculated. Since the random data no longer retain any physical connections between the fundamental variables, the average correlation for these 1000 trials of random data, $\langle R\rangle_{\text{rand}}$, is a measure of self-correlation due to the common divisor. Although there is a superficial resemblance, this method is not the bootstrap method (Efron and Gong 1983).

Original Data				Random			
1:	$\overline{w'\theta'}_1$	u_{*1}	$\partial\overline{U}/\partial z_1$	1:	$\overline{w'\theta'}_6$	u_{*27}	$\partial\overline{U}/\partial z_{14}$
2:	$\overline{w'\theta'}_2$	u_{*2}	$\partial\overline{U}/\partial z_2$	2:	$\overline{w'\theta'}_{48}$	u_{*61}	$\partial\overline{U}/\partial z_{59}$
	⋮	⋮	⋮		⋮	⋮	⋮
N:	$\overline{w'\theta'}_N$	u_{*N}	$\partial\overline{U}/\partial z_N$	N:	$\overline{w'\theta'}_{72}$	u_{*35}	$\partial\overline{U}/\partial z_{10}$

Figure 2. Example of construction of random dataset. See text for explanation.

TABLE 2. SELF-CORRELATION ANALYSIS

Level (m)	N	R_{data}	$\langle R\rangle_{\text{rand}}$	$R^2_{\text{data}} - \langle R^2\rangle_{\text{rand}}$
0.5	45	0.75	0.61	0.17
1.5	34	0.73	0.71	0.02
5	88	0.83	0.65	0.27
10	82	0.85	0.67	0.28
20	77	0.71	0.66	0.06
30	69	0.95	0.67	0.45
40	92	0.92	0.70	0.34
50	86	0.89	0.67	0.35

Linear-correlation coefficient for the original data, R_{data}, and the average correlation coefficients for 1000 trials of random data, $\langle R\rangle_{\text{rand}}$, for each level. $\langle R\rangle_{\text{rand}}$ is the self-correlation and is the adopted reference point of no correlation. Physical percent variance explained by a linear model is approximated by the difference $R^2_{\text{data}} - \langle R^2\rangle_{\text{rand}}$. N is the number of data points.

For CASES99, the randomized data at different levels yield average values for $\langle R\rangle_{\text{rand}}$ of 0.61–0.69 with standard deviations of 0.07–0.13 depending on level. Although the values of R_{data} are quite large (0.71–0.93), they are only modestly larger than the reference point of no physical correlation, $\langle R\rangle_{\text{rand}}$ (Table 2).

(*b*) *Variance explained*

The square of the linear-correlation coefficient is a measure of the percent of the variance in the data that is explained by a linear model (e.g. Snedecor and Cochran 1976). For the present datasets, most of the variance explained for the original data is associated with self-correlation. The difference between the variance explained for the original data, R^2_{data}, and the random data, $\langle R^2\rangle_{\text{rand}}$, is proposed as a measure of the true physical variance associated with the underlying processes governing the turbulence (Table 2). This difference is not a true variance in that it can be negative if the original data correlation, R_{data}, and the self-correlation $\langle R\rangle_{\text{rand}}$ are of opposite sign and R^2_{data} is less than $\langle R^2\rangle_{\text{rand}}$. Such a situation did not occur here.

This measure is not complete since the self-correlation is not necessarily expected to be linear because $\phi_m \propto 1/u_*$ and $z/L \propto 1/u_*^3$. In addition, the physical correlation may not be linear for highly stable conditions. Although the linear correlation coefficient can be sensitive to a few outlying points, we dismiss more sophisticated statistical measures because of difficulties of interpretation and non-generality.

(*c*) *Self-correlation: other datasets*

Because the self-correlation coefficients are large for the CASES99 data, we extended the study to other datasets with adequate estimates of vertical gradients to determine if they yield similar results. Six stable nights in Borris95 provide about

TABLE 3. SELF-CORRELATION ANALYSIS OF BORRIS95 DATA

Level (m)	N	R_{data}	$\langle R\rangle_{\text{rand}}$
7	31	0.77	0.63
10	36	0.91	0.62
20	39	0.83	0.43

Linear-correlation coefficients R_{data} for Borris95 data, and the average linear-correlation coefficients for the random data, $\langle R\rangle_{\text{rand}}$, for each level. N is the number of data points.

TABLE 4. SELF-CORRELATION ANALYSIS OF MICROFRONTS DATA

Level (m)	N	R_{data}	$\langle R\rangle_{\text{rand}}$
3	107	0.92	0.65
10	101	0.88	0.67

See Table 3.

40 hours of data. This two-week field programme was conducted by the Meteorology Department of the Risoe National Laboratory in July 1995 over a 4 km ×4 km area of low heather in the Borris Moor of the central part of the Jutland Peninsula of Denmark. Sonic anemometer data are analysed from three levels: 7 m (Solent Gill), 10 m (Kaijo Denki B) and 20 m (Kaijo Denki B). Mean winds are from cup anemometers at 2, 10 and 20 m. There is insufficient neutral data to estimate z_0. Only data satisfying the conditions outlined in section 4 are considered.

The values for R_{data} for Borris95 are comparable to the CASES99 values. The values of $\langle R\rangle_{\text{rand}}$ are also similar to the CASES99 values, except at 20 m, where it is only 0.43 (Table 3). The data at 20 m sample a broader range of heat fluxes and shears than sampled by the lower instruments, so the $\langle \text{R}\rangle_{\text{rand}}$ value is smaller even though the range of u_* values is similar at all the levels.

The Microfronts field campaign took place over grassland in south central Kansas, late February to March 1995 (Sun 1999). The local-fit wind profiles use cup anemometer data from 3, 5 and 10 m as well as a surface constraint of vanishing wind at $z_0 = 0.03$ m. Sonic anemometers were located at 3 and 10 m. The values for R_{data} and $\langle R\rangle_{\text{rand}}$ are comparable to the CASES99 analysis (Table 4).

6. ADDITIONAL APPROACHES

(*a*) *Self-correlation analysis of subsets of the CASES99 data*

Since $\phi_m = 1 + \beta z/L$ is expected to be most valid at small z/L and may be less accurate for large z/L, the data for each observational level are divided into two subsets: one for z/L less than a cut-off value, the other for z/L greater than a cut-off value. The cut-off value is chosen so that the two subsets have roughly the same number of data points, so a different cut-off value is needed for each observational level (Table 5). The test for self-correlation is repeated for each subset separately.

The R_{data} values are larger for the data with small z/L (Table 5) indicating a better fit to theory for the small z/L data than for the higher stability data. The 10 m level is an exception for unknown reasons. The average random correlations $\langle R\rangle_{\text{rand}}$ are also larger for the small z/L data and smaller for the more stable large z/L data. As a result, the physical variance, $R^2_{\text{data}} - \langle R^2\rangle_{\text{rand}}$, is about the same for both stability categories.

TABLE 5. SELF-CORRELATION ANALYSIS FOR SUBSETS OF CASES99 DATA

		Small z/L			Large z/L		
Level (m)	Cut-off z/L	N_{low}	R_{data}	$\langle R\rangle_{\text{rand}}$	N_{high}	R_{data}	$\langle R\rangle_{\text{rand}}$
0.5	0.08	21	0.84	0.72	24	0.49	0.58
1.5	0.12	19	0.95	0.75	15	0.57	0.72
5	0.50	39	0.96	0.83	49	0.62	0.56
10	0.90	44	0.74	0.80	38	0.79	0.63
20	1.70	36	0.78	0.72	41	0.62	0.61
30	1.30	31	0.94	0.77	38	0.91	0.61
40	1.84	50	0.90	0.75	42	0.89	0.64
50	1.41	46	0.91	0.66	40	0.80	0.54

Linear-correlation coefficient R_{data} for small z/L data (see text) and large z/L data, and the average linear-correlation coefficient for 1000 trials of random data, $\langle R\rangle_{\text{rand}}$, for each subset at each level. N_{low} is the number of data points with z/L less than the cut-off z/L value, N_{high} is the number with z/L more than the cut-off.

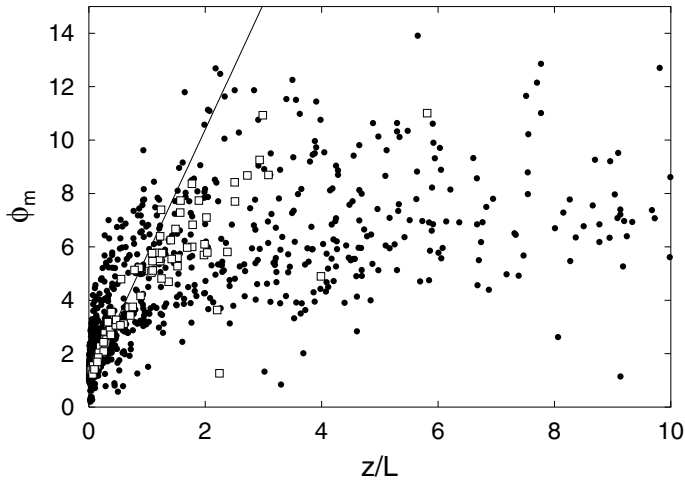

Figure 3. 5 m data and randomized data. The line is $\phi_m = 1 + 4.7(z/L)$, white squares are the 88 points of data, and the dark circles are 900 of the 1000 random points generated from the data. The 100 random data points not shown have $10 < z/L < 60$ and $1.5 < \phi_m < 15$. See text for explanation of symbols.

The small z/L data represent a wider range of u_* values yielding a larger coefficient of variation (section 5) than the large z/L data, resulting in a larger self-correlation $\langle R\rangle_{\text{rand}}$ for the small z/L data.

(*b*) *Large sample of random data*

Apparently, the large fraction of total variance explained by self-correlation is common not just to all three field campaigns, but also to subsets of the data. However, even for the subset analysis, the $\langle R\rangle_{\text{rand}}$ values could be influenced by a small number of very large z/L points generated by the randomization. Therefore, we analyse a single large randomized dataset of 1000 points instead of the ensemble of small randomized datasets (1000 sets of 88 points each). The same random sampling algorithm is used to generate the 1000 random points, here from the 5 m observed data (Fig. 3). The large number of random data points allows a visual sense of the influence of self-correlation.

In spite of substantial scatter in the random data (Fig. 3), the small z/L points cluster nearer the theoretical relationship $\phi_m = 1 + 4.7(z/L)$ than the large z/L points.

Although the random values of ϕ_m are never larger than 15, the random values of z/L become as large as 60. The R value for all 1000 points is 0.65, the same as the ensemble $\langle R\rangle_{\text{rand}}$ value for the same level (Table 2). Approximately 10% of the random data are characterized by $z/L > 10$ while the 88 observed data points are all $z/L < 6$. The ensemble $\langle R\rangle_{\text{rand}}$ values are influenced by these extremely large z/L points. Even using only a weakly stable subset of data to generate the random data, as in the previous subsection, will produce some random data points with large z/L values.

Truncating the large random dataset to exclude $z/L > 6$ yields an R for the remaining 829 points of 0.71 resulting in a physical variance estimate of $R^2_{\text{data}} - \langle R^2\rangle_{\text{rand}} = 0.18$, even smaller than the original estimate of 0.27 in Table 2. Results are similar repeating the ensemble $\langle R\rangle_{\text{rand}}$ analysis but restricting all 88 points in each of the 1000 realizations to $z/L < 6$:

$$\langle R\rangle_{\text{rand}} = 0.69, \quad R^2_{\text{data}} - \langle R^2\rangle_{\text{rand}} = 0.21.$$

Since self-correlation $\langle R\rangle_{\text{rand}}$ was increased by discarding the random data points with extremely large z/L, the quantitative estimate of the self-correlation is subject to some uncertainty. However, truncating the large random dataset or limiting z/L for the ensemble analysis makes the analysis no longer truly random and should be interpreted cautiously.

The 5 m data, plotted with the random data in Fig. 3, show excellent agreement with theory in the range $0 < z/L < 0.5$, and good agreement but increased scatter in the range $0.5 < z/L < 1.0$. As z/L increases further, the observed data become nearly as scattered as the random points. At the other instrument levels, the scatter of the observed data approaches the random points as z/L exceeds a threshold which varies depending on the level. These subjective impressions are difficult to demonstrate objectively (section 6(a)). Self-correlation is evident for all z/L based on the results of Table 2, but is most significant for large z/L (Fig. 3) where the scatter for the original data is as large as that for the randomized data. The decrease of ϕ_m below the linear prediction found in strongly stable data could be due primarily to self-correlation.

7. Conditional analysis of intermittent data

(*a*) *Non-stationarity and intermittency*

Turbulent scaling laws assume stationary conditions, so the non-stationarity due to intermittent turbulence may introduce scatter. Removing subsections of weak turbulence from each hour might reduce the scatter. The low-turbulence subsegments were too contaminated by trend due to mesoscale motions to confidently analyse the data. With very weak turbulence signals, even modest mesoscale trend becomes important. Using the same hours of data as used for section 5 and Table 2, for each hour, a 100 s section of data was considered turbulent if $\sigma_w > 0.05$ m s^{-1}. The 1-hour average flux is taken as the average over all the turbulent sections of that hour. Each hour has at least 10 min (six 100 s segments) of data above the threshold. This removal of low-turbulence sections from each hour reduces the non-stationarity due to intermittency. This method differs from the technique in section 4 where entire hours were rejected as being below threshold.

Conditional gradients are computed from locally fitted 100 s gradients based on 100 s values of $\overline{U}$. The 1-hour gradient is taken as the average of only those 100 s gradients from the turbulent sections of that hour. For the fully turbulent hours, this

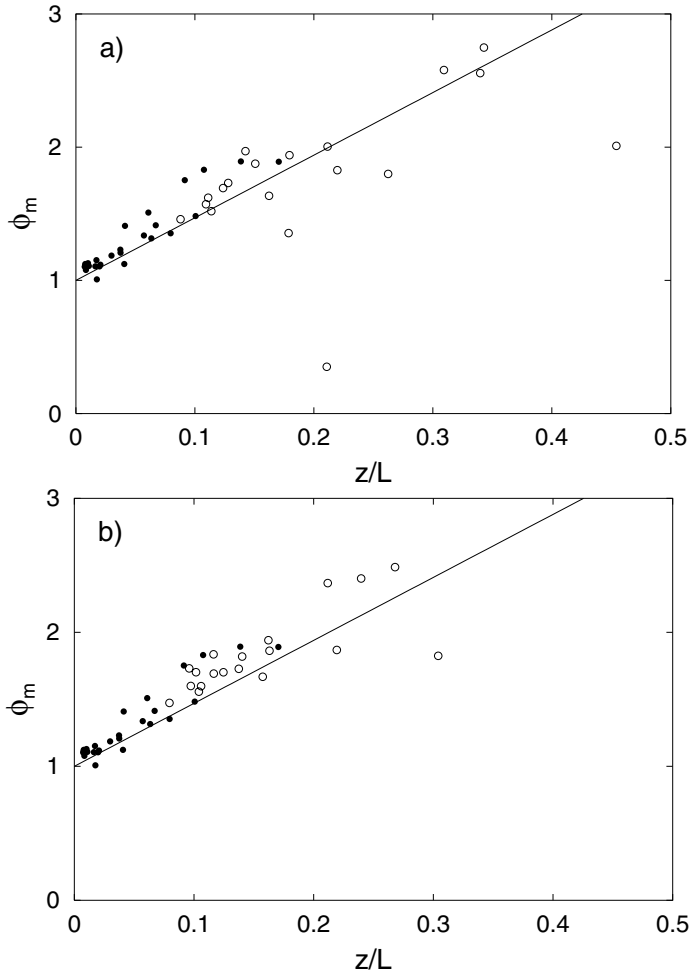

Figure 4. (a) Traditional and (b) conditional analysis of 0.5 m CASES99 data. The line is $\phi_m = 1 + 4.7(z/L)$, open circles are intermittent data, filled circles are non-intermittent data that do not change with conditional analysis. See text for meaning of symbols.

method produces the same gradient as the conventional method of using the 1-hour mean wind to calculate the 1-hour gradient.

(*b*) *Influence on scaling laws*

The conditional analysis tends to significantly move the outlying points in the relationship between ϕ_m and z/L towards the theoretical relationship as well as move many of the other points a small distance towards the theoretical relationship. These adjustments are mostly due to reduced z/L (compare panels (a) and (b) in Figs. 4 and 5). Both u_*^2 and $\overline{w'\theta'}$ increase by about the same percentage with application of conditional analysis, resulting in decreased z/L since L is proportional to u_*^3.

Conditional analysis increases R_{data} most dramatically at 0.5 and 1.5 m (Table 6). At these levels, conditional analysis increases the shear more than at the other levels. The physical percent variance explained increases substantially at the lower levels owing to conditional analysis, less so at higher levels.

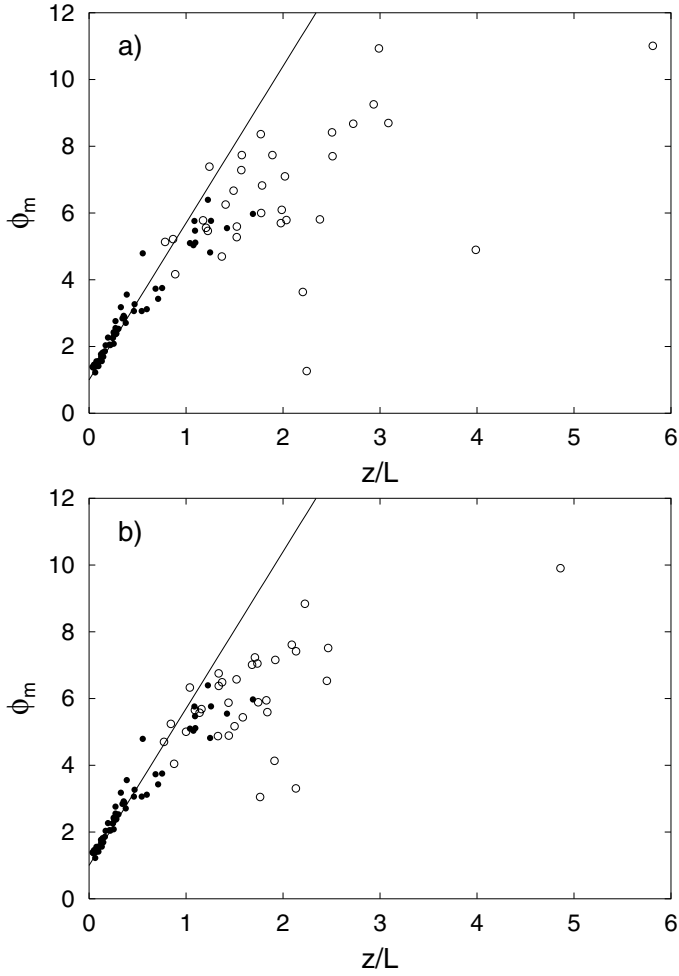

Figure 5. As Fig. 4, but for 5 m CASES99 data.

TABLE 6. SELF-CORRELATION ANALYSIS OF CONDITIONAL DATA

Level (m)	N	R_{data}	$\langle R\rangle_{\text{rand}}$	$R^2_{\text{data}} - \langle R^2\rangle_{\text{rand}}$
0.5	45	0.91	0.64	0.41
1.5	34	0.97	0.73	0.41
5	88	0.88	0.65	0.34
10	82	0.82	0.67	0.22
20	77	0.84	0.64	0.30
30	69	0.96	0.67	0.47
40	92	0.90	0.69	0.34
50	86	0.96	0.68	0.45

Linear-correlation coefficient R_{data} for conditional data and the average correlation coefficients for 1000 trials of random data, $\langle R\rangle_{\text{rand}}$, for each level. $\langle R\rangle_{\text{rand}}$ is the self-correlation and is the adopted reference point of no correlation. Physical percent variance explained by a linear model is approximated by the difference $R^2_{\text{data}} - \langle R^2\rangle_{\text{rand}}$. N is the number of data points.

Conditional analysis most affects the data points with very stable, weak-wind conditions. The CASES99 data, as well as the Borris95 and Microfronts data, have many more hours with significant wind and weak stability than hours with weak winds. Conditional analysis may have a larger effect for data dominated by weak-wind very stable conditions with more extensive intermittency.

(*c*) *Sensitivity to σ_w threshold value and σ_w averaging window*

Sensitivity of the conditional analysis to the σ_w threshold value is now investigated. Repeating the conditional analysis with different threshold values finds that the linear-correlation coefficients for the conditional data change by only about 5% over a range of 0.040 m s^{-1} $< \sigma_w <$ 0.100 m s^{-1} at all the observational levels except the 0.5 m level where R values vary by as much as 12% over the same range of σ_w. We are using $\sigma_w = 0.05$ m s^{-1} as the threshold for this study.

Using short 100 s averaging windows to compute the conditional fluxes also allows the conditional analysis to capture more detail of the intermittency compared to using longer averaging windows. Repeating the analysis, using 1 min blocks of data to compute σ_w and the conditional fluxes, yields results nearly identical to using 100 s blocks. Windows shorter than about one minute do not capture enough turbulent flux to be meaningful even for highly stable conditions. Using 5 min blocks results in more scatter for both conditional and traditional data, the hours with small flux values being most affected. The perturbations computed as deviations from longer averages are more contaminated by mesoscale motions (Vickers and Mahrt 2003).

8. z-LESS ANALOG TO MONIN–OBUKHOV SIMILARITY THEORY

Self-correlation is difficult to avoid because most scaling schemes, in order to maintain simplicity, deliberately use a limited number of fundamental variables, requiring the use of at least one of the fundamental variables in more than one of the resulting dimensionless terms. This section evaluates the relative impact of self-correlation on z-less similarity theory. To derive z-less similarity theory, one must assume that the turbulence is stationary and not influenced by advection, the shear and wind vectors are aligned, and that important additional length-scales are not introduced by curvature of the temperature and wind profiles, as might occur with a low-level jet. Only conditional data have been used in the following analysis as they yield less scatter compared to the original data (section 7).

(*a*) *Application of Buckingham Pi formalism*

Similar to the derivation of Monin–Obukhov similarity theory in section 2, an analogous pair of z-less Pi groups can be derived using

$$\overline{w'\theta'}, \quad u_* = (\overline{u'w'}^2 + \overline{v'w'}^2)^{1/4}, \quad \partial\overline{U}/\partial z, \quad \partial\overline{\theta}/\partial z \quad \text{and} \quad g/\overline{\theta}$$

as the relevant variables. Here, $\overline{w'\theta'}$ and u_* are the local fluxes at height z, not the surface fluxes. These fundamental variables do not include z or the surface fluxes, so the derivation is applicable to very stable conditions when the turbulence has become partially decoupled from the surface and no longer directly related to the surface values (Derbyshire 1999; Mahrt and Vickers 2003, and references therein). The constraints put on this set of variables by Buckingham Pi theory will yield only two independent Pi groups (e.g. Stull 1988; Barenblatt 1996).

The terms, which comprise the two Pi groups, can be rearranged into a variety of combinations. One familiar pair of Pi groups is

$$\left(\frac{g}{\theta}\frac{\partial\overline{\theta}}{\partial z}\right) \Bigg/ \left(\frac{\partial\overline{U}}{\partial z}\right)^2 \equiv Ri, \tag{3}$$

$$\frac{\kappa L}{u_*}\frac{\partial\overline{U}}{\partial z} \equiv \phi'_m, \tag{4}$$

where L is explicitly calculated from local flux values as

$$L = \frac{-\overline{\theta}}{\kappa g}\frac{u_*^3}{\overline{w'\theta'}}. \tag{5}$$

The first Pi group is the gradient Richardson number and the second is a dimensionless shear analogous to ϕ_m (Eq. (2)); ϕ'_m is also the inverse of the flux Richardson number. These equations are z-less in that no dependence on z or the boundary-layer depth appear. This pair of Pi groups is not unique. Another possible pair is Ri and $\phi'_h \equiv (\kappa L/\theta_*)(\partial\overline{\theta}/\partial z)$.

The formalism of Buckingham Pi theory states that if only two independent Pi groups exist, one must be a function of the other as long as the variables chosen as the relevant variables are the primary variables governing the flow. In other words, the dimensionless shear must be a function of only the gradient Richardson number or vice versa. Buckingham Pi theory does not give any indication of what that function might be, so it must be determined experimentally.

In this case, K theory provides insight into the relationship between Ri and ϕ'_m. Since ϕ'_m is the inverse of the flux Richardson number and Ri is the gradient Richardson number, application of K theory yields an expression for ϕ'_m in terms of the inverse of Ri.

$$\phi'_m = R_f^{-1} = \frac{-u_*^2}{(g/\overline{\theta})\overline{w'\theta'}}\left(\frac{\partial\overline{U}}{\partial z}\right) = \frac{-K_m(\partial\overline{U}/\partial z)}{-(g/\overline{\theta})K_h(\partial\overline{\theta}/\partial z)}\left(\frac{\partial\overline{U}}{\partial z}\right) = \frac{K_m}{K_h}Ri^{-1}, \tag{6}$$

where K_m and K_h are the eddy diffusivity for momentum and heat, respectively, and R_f is the flux of Richardson number.

The turbulent Prantl number K_m/K_h is often taken to be 1.0 in the surface layer. Most of our data support $K_m/K_h = 1.0$, corresponding to a slope of unity in Fig. 6. In general, the data would be plotted in the form of R_f vs. Ri, but this derivation using Buckinham Pi formalism instructs us to also look at other ways to plot the data: ${R_f}^{-1}$ vs. Ri; R_f vs. Ri^{-1}; ${R_f}^{-1}$ vs. Ri^{-1}. On the traditional R_f vs. Ri plots, the data support $K_m/K_h = 1.0$. On the plots using ${R_f}^{-1}$ vs. Ri^{-1}, the data that were clustered near the origin on R_f vs. Ri plots (near-neutral data), are now spread out making it easier to visualize the deviation of the near-neutral data from $K_m/K_h = 1.0$. However, for the near-neutral data, Monin–Obukhov similarity theory performs well, implying that z is an important variable and that the above z-less analysis does not apply.

It is unknown why some of the data lie along the $K_m/K_h = 0.4$ line. Although conservative estimates of the measurement uncertainties do not support $K_m/K_h = 1$ for these subsets, we can not rule out simultaneous overestimation of shear and underestimation of the temperature gradient for this subset. Such errors would act to systematically increase Ri^{-1}. However, for these weakly stable cases, Monin–Obukhov similarity theory or local similarity may perform well, implying that z is an important variable and that the above z-less analysis is incomplete.

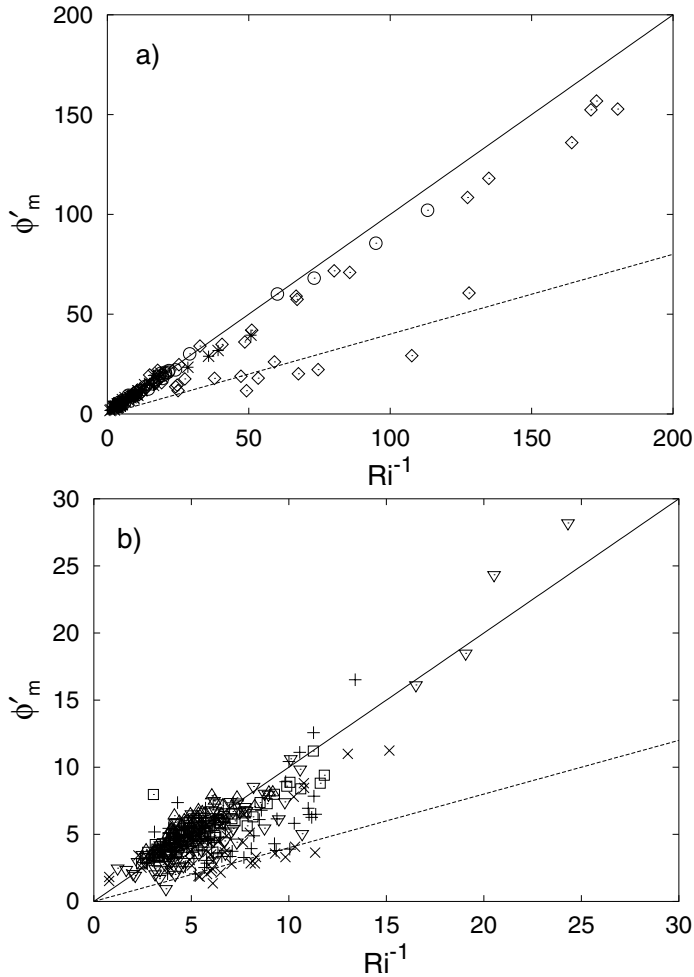

Figure 6. ϕ'_m as a function of Ri^{-1}. The slope is K_m/K_h. The solid lines are $K_m/K_h = 1$, the dashed lines are $K_M/K_H = 0.4$. (a) Data for 0.5 m (◇), 1.5 m (○) and 5 m (∗). (b) Data for 10 m (▽), 20 m (×), 30 m (△), 40 m (+), 50 m (□). See text for explanation of symbols.

(*b*) *Self-correlation*

Since $\partial\overline{U}/\partial z$ occurs in both terms, this relationship is also subject to self-correlation. The average linear-correlation coefficients for the data range from 0.61–0.99 for the original data and 0.03–0.14 for the randomized data (Table 7), as compared to 0.6–0.7 (Table 6) for Monin–Obukhov similarity theory or local similarity theory. The small self-correlation is due to the fact that the range of shear data is relatively small compared to the range of the turbulent fluxes (section 5). The largest range of shear values is found at the lowest levels and is reflected in the larger $\langle R\rangle_{\text{rand}}$ values at 0.5 and 1.5 m. Monin–Obukhov similarity is much more vulnerable to self-correlation than the z-less theory previously described due to the large range of the common variable u_*.

TABLE 7. SELF-CORRELATION ANALYSIS OF z-LESS SCALING

Level (m)	N	R_{data}	$\langle R\rangle_{\text{rand}}$	$R^2_{\text{data}} - \langle R^2\rangle_{\text{rand}}$
0.5	45	0.93	0.14	0.85
1.5	28	0.998	0.10	0.986
5	80	0.985	0.03	0.97
10	75	0.94	0.04	0.88
20	67	0.63	0.05	0.39
30	59	0.83	0.06	0.69
40	82	0.61	0.05	0.37
50	76	0.88	0.07	0.77

Linear-correlation coefficient R_{data} for shear ϕ'_m as a function of Ri^{-1} and the average correlation coefficients for 1000 trials of random data, $\langle R\rangle_{\text{rand}}$ and the estimate of the percent physical variance explained, $R^2_{\text{data}} - \langle R^2\rangle_{\text{rand}}$. $\langle R\rangle_{\text{rand}}$ is the amount of correlation due to self-correlation and is the reference point of no correlation rather than $R = 0$.

9. CONCLUSIONS

For stable conditions, self-correlation contributes significantly to the linear-correlation coefficient between the non-dimensional shear ϕ_m and z/L owing to the occurrence of u_* in both terms. The self-correlation, as measured by the average linear-correlation coefficient for randomized data, was found to be significantly larger than zero and typically not small compared to the linear correlation for the original data. Self-correlation was large for the entire range of stability and was large whether Monin–Obukhov similarity was valid or whether only local similarity theory was valid. Subjective examination of actual data compared to a large sample of randomized data seems to imply an excellent fit of the near-neutral data to the linear theory, but an unexpectedly large self-correlation for near-neutral conditions made this impression difficult to support objectively. Although the estimate of self-correlation is itself an uncertain process, we conclude that substantial physical correlation can not be established for our three stable boundary-layer datasets.

While the physical correlation (excess correlation beyond self-correlation) between ϕ_m and z/L is generally much smaller than the total correlation, linear-correlation analysis may be incomplete. There is a need to develop a better statistical approach that will objectively quantify the effects of self-correlation. Furthermore, the correlation may be reduced by observational errors especially for very stable conditions. The self-correlation for z-less similarity theory based on the Richardson number was much less than that for Monin–Obukhov similarity theory, although still significant near the ground surface.

Removal of record subsections corresponding to very weak turbulence (conditional analysis) improves the flux–gradient relationship and reduces non-stationarity such that the conditions required for similarity are likely to be met. With such restrictions, similarity theory explains significantly more of the variance of ϕ_m, depending on observational level. Such conditional analysis may show more dramatic reductions in scatter for data more dominated by intermittent turbulent conditions (weaker winds).

ACKNOWLEDGEMENTS

We gratefully acknowledge the field assistance of the National Centers for Atmospheric Research ATD staff, Jielun Sun and Sean Burns in CASES99 and the comments of two anonymous reviewers. Hans Jørgensen provided the data from Borris95. This material is based upon work supported by Grant DAAD19-0210224 from the Army

Research Office and Grant 0107617-ATM from the Physical Meteorology Program of the National Sciences Program. Thanks to Dean Vickers of Oregon State University for the roughness-length calculations.

REFERENCES

Aldrich, J. 1995 Correlations genuine and spurious in Pearson and Yule. *Statistical Science*, **10,** 364–376

Andreas, E. L. 2002 Parameterizing scalar transfer over snow and ice: A review. *J. Hydrometeorol.*, **3,** 417–431

Banta, R. M., Newsom, R. K., Lundquist, J. K., Pichugina, Y. L., Coulter, R. L. and Mahrt, L. 2002 Nocturnal low-level jet characteristics over Kansas during CASES99. *Boundary-Layer Meteorol.*, **105,** 221–252

Barenblatt, G. I. 1996 *Scaling, self-similarity, and intermediate asymptotics*. Cambridge University Press

Beljaars, A. C. M. and Holtslag, A. A. M. 1991 Flux parameterization over land surfaces for atmospheric models. *J. Appl. Meteorol.*, **30,** 327–341

Derbyshire, S. H. 1999 Boundary-layer decoupling over cold surfaces as a physical boundary-instability. *Boundary-Layer Meteorol.*, **90,** 297–325

Efron, B. and Gong, G. 1983 A leisurely look at the bootstrap, the jackknife, and cross-validation. *The American Statistician*, **37,** 36–48

Finnigan, J. J. and Einaudi, F. 1981 The interaction between an internal gravity wave and the planetary boundary layer. Part II: Effect of the wave on the turbulence structure. *Q. J. R. Meteorol. Soc.*, **107,** 807–832

Hicks, B. B. 1978a Some limitations of dimensional analysis and power laws. *Boundary-Layer Meteorol.*, **14,** 567–569

1978b Comments on 'The characteristics of turbulent velocity components in the surface layer under convective conditions', by H. A. Panofsky, H. Tennekes, D. H. Lenschow and J. C. Wyngaard. *Boundary-Layer Meteorol.*, **15,** 255–258

1981 An examination of turbulence statistics in the surface boundary layer. *Boundary-Layer Meteorol.*, **21,** 389–402

Högström, U 1988 Non-dimensional wind and temperature profiles in the atmospheric surface layer: A re-evaluation. *Boundary-Layer Meteorol.*, **42,** 55–78

1996 Review of some basic characteristics of the atmospheric surface layer. *Boundary-Layer Meteorol.*, **78,** 215–246

Holtslag, A. A. M. and De Bruin, H. A. R. 1988 Applied modeling of the nighttime surface energy balance over land. *J. Appl. Meteorol.*, **27,** 689–704

Howell, J. and Sun, J. 1999 Surface layer fluxes in stable conditions. *Boundary-Layer Meteorol.*, **90,** 495–520

Kim, J.-H. 1999 Spurious correlation between ratios with a common divisor. *Statistics and Probability Letters*, **44,** 383–386

Mahrt, L. and Vickers, D 2003 Formulation of turbulent fluxes in the stable boundary layer. *J. Atmos. Sci.*, **60,** 2538–2548

Mahrt, L., Vickers, D., Frederickson, P., Davidson, K. and Smedman, A.-S. 2003 Sea-surface aerodynamic roughness. *J. Geophys. Res.*, **108,** 1–9

Nieuwstadt, F. 1984 The turbulent structure of the stable, nocturnal boundary layer. *J. Atmos. Sci.*, **41,** 2202–2216

Poulos, G. S., Blumen, W., Fritts, D. C., Lundquist, J. K., Sun, J., Burns, S. P., Nappo, C., Banta, R., Newsome, R., Cuxart, J., Terradellas, E., Balsley, B. and Jensen, M. 2002 CASES-99: A comprehensive investigation of the stable nocturnal boundary layer. *Bull. Am. Meteorol. Soc.*, **83,** 555–581

Snedecor, G. and Cochran, W. 1976 *Statistical methods*. The Iowa State University Press, Ames, Iowa, USA

Soler, M. R., Infante, C., Buenestado, P. and Mahrt, L. 2002 Observations of nocturnal drainage flow in a shallow gully. *Boundary-Layer Meteorol.*, **105,** 253–273

Sorbjan, Z. 1989 *Structure of the atmospheric boundary layer*. Prentice-Hall, Englewood Cliffs, New Jersey, USA

Stull, R. B. 1988 *An Introduction to boundary-layer meteorology*. Kluwer Academic Publishers, Boston, Massachusetts, USA

Sun J. 1999 Diurnal variation of thermal roughness height over a grassland. *Boundary-Layer Meteorol.*, **92,** 407–427

Sun, J., Burns, S. P., Lenschow, D. H., Banta, R., Newsom, R., Coulter, R., Frasier, S., Ince, T., Nappo, C., Cuxart, J., Blumen, W., Lee, X. and Hu, X.-Z. 2002 Intermittent turbulence associated with a density current passage in the stable boundary layer. *Boundary-Layer Meteorol.*, **105,** 199–219

Vickers, D. and Mahrt, L. 1999 Observations of non-dimensional wind shear in the coastal zone. *Q. J. R. Meteorol. Soc.*, **125,** 2685–2702

2003 The cospectral gap and turbulent flux calculations. *J. Atmos. Oceanic Technol.*, **20,** 660–672